View metadata, citation and similar papers at core.ac.uk

brought to you by CORE

provided by University of Central Florida (UCF): STARS (Showcase of Text, Archives, Research &...

University of Central Florida

STARS

Faculty Bibliography 2000s

Faculty Bibliography

1-1-2008

Defects and symmetry influence on visible emission of Eu doped nanoceria

Suresh Babu
University of Central Florida

Alfons Schulte
University of Central Florida

Sudipta Seal
University of Central Florida

Find similar works at: https://stars.library.ucf.edu/facultybib2000
University of Central Florida Libraries http://library.ucf.edu

This Article is brought to you for free and open access by the Faculty Bibliography at STARS. It has been accepted for inclusion in Faculty Bibliography 2000s by an authorized administrator of STARS. For more information, please contact STARS@ucf.edu.

Recommended Citation

Babu, Suresh; Schulte, Alfons; and Seal, Sudipta, "Defects and symmetry influence on visible emission of Eu doped nanoceria" (2008). *Faculty Bibliography 2000s*. 90.
https://stars.library.ucf.edu/facultybib2000/90

Applied Physics Letters

Defects and symmetry influence on visible emission of Eu doped nanoceria

Cite as: Appl. Phys. Lett. **92**, 123112 (2008); https://doi.org/10.1063/1.2904627
Submitted: 19 January 2008 . Accepted: 10 March 2008 . Published Online: 28 March 2008

Suresh Babu, Alfons Schulte, and Sudipta Seal


View Online


Export Citation

ARTICLES YOU MAY BE INTERESTED IN

Size dependency variation in lattice parameter and valency states in nanocrystalline cerium oxide
Applied Physics Letters **87**, 133113 (2005); https://doi.org/10.1063/1.2061873

Cerium oxide nanoparticles: Size-selective formation and structure analysis
Applied Physics Letters **80**, 127 (2002); https://doi.org/10.1063/1.1430502

Role of trivalent La and Nd dopants in lattice distortion and oxygen vacancy generation in cerium oxide nanoparticles
Applied Physics Letters **88**, 243110 (2006); https://doi.org/10.1063/1.2210795

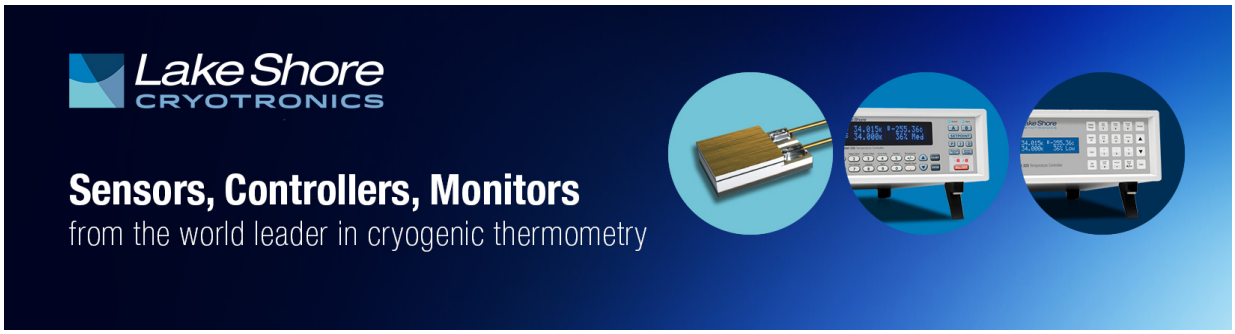

© 2008 American Institute of Physics.

Defects and symmetry influence on visible emission of Eu doped nanoceria

Suresh Babu,[1] Alfons Schulte,[2] and Sudipta Seal[1,a)]
[1]*Advanced Materials Processing and Analysis Centre (AMPAC), Nanoscience Technology Center and Mechanical, Materials and Aerospace Engineering (MMAE), University of Central Florida, 4000 Central Florida Boulevard, Orlando, Florida 32816, USA*
[2]*Department of Physics, University of Central Florida, 4000 Central Florida Boulevard, Orlando, Florida 32816, USA*

(Received 19 January 2008; accepted 10 March 2008; published online 28 March 2008)

Europium doped cerium oxide particles of 10 nm were synthesized by room temperature chemical precipitation technique and annealed at 500 and 900 °C to study its effect on luminescence. X-ray photoelectron spectroscopic result shows an increase in Ce^{3+} concentration from 20% to 23% on Eu doping but decreases to 8% on annealing. Raman studies show a progressive blueshift from 461 to 464 cm^{-1} due to local symmetry ordering with temperature. Emission intensity varies with the wavelength of excitation and observed transitions indicate the presence of Eu^{3+} in different symmetry environments. © *2008 American Institute of Physics*. [DOI: 10.1063/1.2904627]

Nanostructures of rare-earth cerium oxide or ceria (CeO_2) have a wide range of applications such as electrolyte in solid oxide fuel cell, oxygen gas sensors, chemical polishing, and catalyst. Recently, beneficial therapeutic properties of ceria nanoparticles have been reported.[1] Since ceria exhibits weak luminescence, doping with rare earths such as europium (Eu) can enhance the visible emission required for imaging. Although emission properties of Eu doped in various matrices have been studied,[2,3] only a few have been attempted in ceria. Synthesis of Eu doped in ceria by sol-gel[4] and high temperature reaction[5] have been reported. However, characteristic Eu^{3+} emission was not observed for 3.5 nm nanocrystals prepared by nonhydrolytic solution route.[6] In the present communication, we report a simple room temperature technique for the synthesis of Eu doped ceria nanoparticles and correlate the influence of surface and structural symmetries on luminescence characteristics as a function of annealing temperature.

Europium doped (5 wt %) nanoceria was synthesized from the aqueous cerium nitrate hexahydrate (Aldrich, 99%) and europium nitrate trihydrate (Aldrich, 99%) solutions by hydrolysis with ammonia. Resultant powders were washed with water and dried at 100 °C overnight. Similar procedure was used for preparing ceria nanoparticles (C). Eu doped ceria nanoparicles were coded as CE, CE-500, and CE-900 for Eu doped ceria, 500 and 900 °C heat treated samples, respectively (Table I). The powders were characterized using high resolution transmission electron microscopy (HRTEM), x-ray diffraction (XRD), x-ray photoelectron spectroscopy (XPS), Raman, and infrared (IR) spectroscopy.

The HRTEM images were obtained with Philips Tecnai F30 at an operational voltage of 300 keV. The bright field HRTEM images of C, CE, and CE-500 shown in Fig. 1 exhibit nearly spherical 7–13 nm particles, with lattice fringes corresponding to the stable (111) plane. However, CE-900 consists of agglomerate with a mean particle size of 37 nm. On annealing to 900 °C, individual nanoparticles come in contact and align to form octahedral shape in order to minimize the interfacial energy.[7]

The crystal structure was determined with XRD (Rigaku) using Cu Kα radiation. Figure 2(a) shows the XRD pattern for nanoparticles. Reflections can be indexed to fluorite structure of CeO_2 (Ref. 8). The lattice parameter of C was found to be 0.5418 nm, higher than that reported for bulk ceria (0.541 nm). Due to the difference in ionic radii between Ce^{3+} (0.1283 nm) and Ce^{4+} (0.1098 nm), the lattice parameter of C is higher than that of bulk ceria.[9] Since Eu has higher ionic radii (0.121 and 0.126 nm for Eu^{3+} and Eu^{2+}, respectively) than Ce^{4+}, doping of Eu (CE) increases the lattice parameter to 0.5422 nm, which decreases upon annealing.[8] The observed broadness in the XRD peaks can be influenced by size as well as strain of the particles. Williamson–Hall plots were used to separate the effects of size and strain in the nanoparticles using

$$\beta = \beta_{\text{size}} + \beta_{\text{strain}} = \frac{0.9\lambda}{t\cos\theta} + \frac{4(\Delta d)\sin\theta}{d\cos\theta},$$

where β is the full width half maximum of the diffraction peaks after correcting for instrumental broadening, λ is the wavelength of the incident x ray, θ is the diffraction angle, t is the crystal size, and Δd is the difference of the d spacing corresponding to a typical peak. After correcting the instrumental broadening, a plot of $\beta\cos\theta$ against $4\sin\theta$ yields the crystal size from the intercept value and the strain ($\Delta d/d$) from the slope. With annealing temperature, mean crystallite size increases to 39.2 nm at 900 °C with a corresponding

TABLE I. Size, strain and Ce^{3+} concentration for nanoparticles.

Sample	Wt % of Eu	Annealing temperature (°C)	Size (nm)	Strain	Lattice parameter (nm)	Ce^{3+} concentration (%)
C	···	···	9.6	8.5×10^{-3}	0.5418	20
CE	5	···	10.1	9.9×10^{-3}	0.5422	23
CE-500	5	500	12.9	5.3×10^{-3}	0.5413	13
CE-900	5	900	39.2	7.9×10^{-4}	0.5412	8

a)Electronic mail: sseal@mail.ucf.edu.

 © 2008 American Institute of Physics

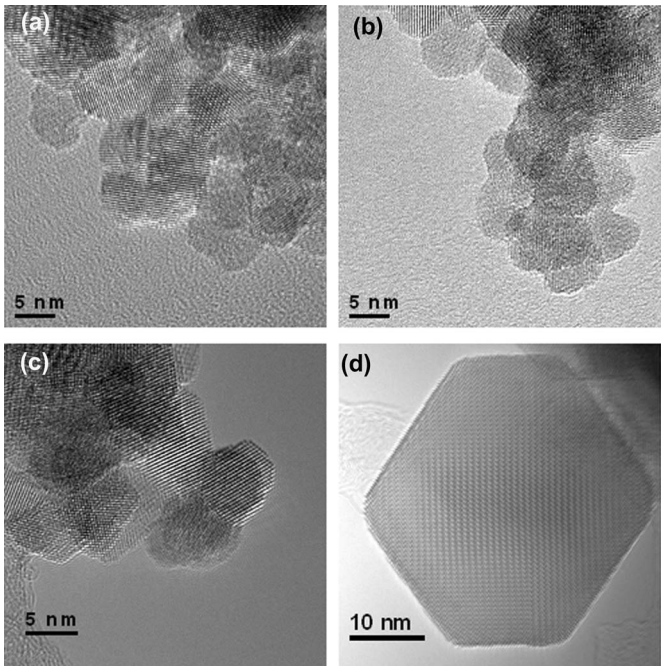

FIG. 1. HRTEM images of (a) C, (b) CE, (c) CE-500, and (d) CE-900.

decrease in strain due to lattice ordering (Table I).

In order to identify the oxidation state of Ce and Eu, XPS study was carried out with Perkin–Elmer (PHI 5400 ESCA) spectrometer. Figure 2(b) shows the recorded spectra for nanoparticles and deconvoluted peaks were used for calculating the concentration of Ce^{3+} (Table I), as reported earlier.[10,11] The concentration of Ce^{3+} increases on doping with Eu^{3+} but decreases on annealing due to the conversion of Ce^{3+} to Ce^{4+}. The inset of Fig. 2(b) shows XPS spectra for Eu 3*d* showing two characteristic peaks at 1134 and 1163 eV corresponding to +3 state and the absence of low binding energy peaks suggest that Eu is present in the +3 state.[12]

Raman scattering is a useful technique to detect oxygen sublattice distortions as electron-phonon (lattice vibration) interactions are very sensitive to local environments. Raman spectroscopic studies were carried out with a Horbia Jobin Yvon LabRam IR micro-Raman system with a He–Ne laser at 632.8 nm. Bulk ceria among the Raman allowed modes exhibits a symmetric, sharp peak centered at 465 cm^{-1} corresponding to a breathing (phonon) mode of O^{2-} anions around Ce^{4+} cation, which are sensitive to any disorder in the oxygen sublattice resulting from nonstoichiometry.[13] Figure 2(c) shows the Raman spectra for all samples. Ceria nanoparticle (C) shows a broad asymmetric peak at a lower frequency of 461 cm^{-1} than bulk ceria due to smaller particle size, which generates larger defect concentration.[14] On annealing, peaks get sharper and symmetric, with a progressive shift in the position from 461 (CE), 462 (CE-500), and 464 cm^{-1} (CE-900). The decrease in the asymmetry is attributed to the improved phonon lifetime due to the growth in nanocrystal size.[13] Annealing reduces the structural gradient induced by the surface strain of nanoparticles. Oxygen vacancies from the bulk of the particle become unstable and tend to migrate to the surface and annihilate, as shown by a decrease in Ce^{3+} concentration in the XPS results. To understand the role of surface chemical modifications, IR spectra were recorded using Perkin–Elmer Spectrum one. IR spectra of ceria and Eu doped ceria samples exhibit a broad peak centered around 3400 cm^{-1} correspond to the O–H symmetric stretching from the surface hydroxyl group due to basic conditions used [Fig. 2(d)] and the reaction can be represented as

$$Ce^{3+} + 3OH^- \rightarrow Ce(OH)_3,$$

$$Ce(OH)_3 + H_2O \rightarrow Ce(OH)_4 + H^+ + e^-,$$

$$Ce(OH)_4 \rightarrow CeO_2 + 2H_2O.$$

As a result of surface dehydroxylation on annealing, OH group intensity decreases for CE-500 and CE-900.

To evaluate the emission characteristics, luminescence measurement were carried out using Hitachi-7000 spectro-

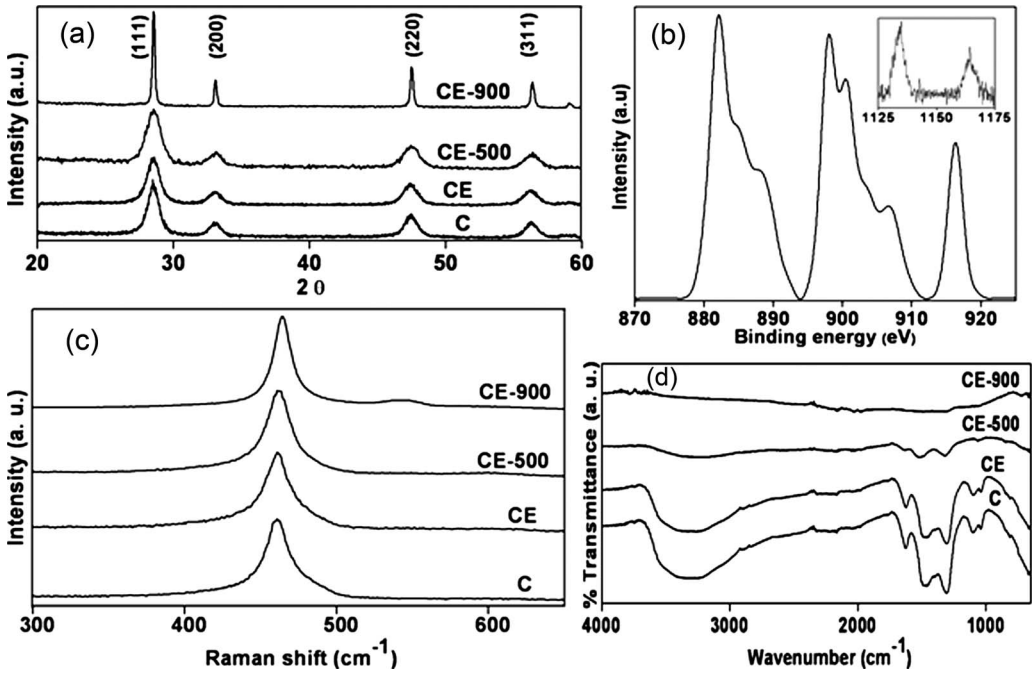

FIG. 2. (a) XRD spectra of nanoparticles. (b) Representative Ce and Eu (inset) 3*d* level XPS spectra of CE. (c) Raman and (d) IR spectra of nanoparticles.

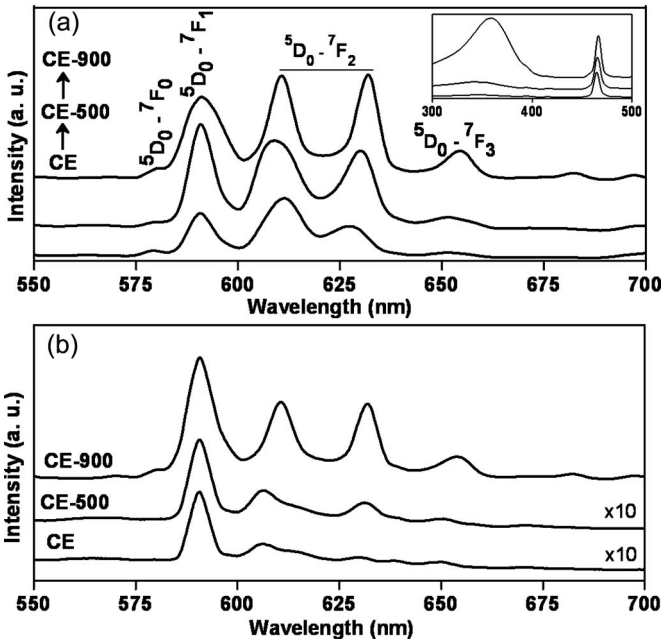

FIG. 3. Emission spectra of nanoparticles excited at 466 (a) and 370 nm (b). The inset shows excitation spectra (λ_{em}=611 nm).

photometer. The inset of Fig. 3(a) shows excitation spectra followed at emission wavelength of 611 nm. The sharp peak at 466 nm corresponds to Eu $4f$-$4f$ transition, and the broad peak results from the overlap between Ce^{4+}–O^{2-} charge transfer and intraconfigurational Eu $4f$-$4f$ transitions. Figure 3(a) shows the characteristic Eu^{3+} emission $^5D_0$-^7F_J (J=0,1,2, etc.) for nanoparticles excited at 466 nm. The emission corresponds to $^5D_0$-$^7F_0$ (579 nm), $^5D_0$-$^7F_1$ (591 nm), $^5D_0$-$^7F_2$ (611 and 632 nm), and $^5D_0$-$^7F_3$ (654 nm) transitions. The $^5D_0$-$^7F_1$ lines originate from the magnetic dipole (MD) transition, while $^5D_0$-$^7F_2$ lines originate from electric dipole (ED) transition. According to the Judd–Ofelt theory, ED transition is only allowed in the absence of inversion symmetry, and is sensitive to the local electric field.[3] CeO_2 has a fluorite structure with Ce located in octahedral symmetry. When Eu^{3+} ions locate at sites with inversion symmetry, MD transition occurs; otherwise, ED transition dominates. The splitting of electric field sensitive $^5D_0$-$^7F_2$ transition indicates that Eu^{3+} exists in at least two structural environments differing in symmetry. The low intensity of $^5D_0$-$^7F_0$ line is due to the fact that this transition is forbidden by both ED and MD selection rules.

The emission mechanism of rare earth-doped materials is generally through energy transfer from the excited host to the dopant and/or direct charge carrier trapping by the dopant molecule. Emission spectrum of nanoparticles excited near the band edge of ceria (370 nm) (Ref. 15) is shown in Fig. 3(b). The emission spectra show strong 591 nm peak while direct Eu^{3+} excitation at 466 nm shows less intense peak at 591 nm than at 611 and 632 nm, indicating the difference in the energy transfer mechanism. On excitation at 370 nm, energy transfer from host to Eu^{3+} occurs, which becomes efficient on annealing. Li *et al.*[16] correlated the electronegativity of rare earth on dehydroxylation with temperature, and Tsunekawa *et al.*[11] observed that in the nanodomain, the surface of the particle predominantly has OH termination rather than O_2^{2-}. Higher electronegativity of Eu^{3+} over Ce^{3+} leads to stronger binding with the surface hydroxyl group, resulting in higher Eu^{3+} concentration on the surface or subsurface. Hydroxyl groups provide an effective pathway for the radiationless energy transfer of OH vibration and quench the emission intensity in the as prepared conditions (CE). Annealing reduces OH groups, leading to an enhanced $^5D_0$-$^7F_2$ emission. The ratio of ED to MD transition increases with temperature as a result of stronger Eu–O covalent bond. Since Ce can exist in +3 and +4 oxidation states, coexistence of (Ce^{3+}–O–Eu^{3+}) and (Ce^{4+}–O–Eu^{3+}) arrangements in the crystalline environment is possible. On annealing, Ce^{4+} concentration increases; this leads to predominant (Ce^{4+}–O–Eu^{3+}) arrangement. Smaller positive charge makes Ce^{4+} more electronegative, leading to more covalent character of Eu–O bond resulting in enhanced ED transition.

In summary, Eu doped ceria nanoparticles were synthesized by room temperature wet chemical precipitation technique. Size of the particles increased from 10 to 39 nm on annealing with retained fluorite structure. The ratio of Ce^{4+} to Ce^{3+} is one of the important factors in determining the Eu^{3+} emission. A reduction in the surface hydroxyl, defect, and Ce^{3+} concentration results in enhanced emission intensity. Depending on the wavelength of excitation, emission pattern varies due to the difference in energy transfer mechanisms. The present result shows that the local chemical environments, as well as defects, have a strong influence on the luminescence properties of nano rare earth emitters.

This research (various sections) is funded by NSF NIRT CBET: 0708172, NSF CMII: 0629080, and NSF MRI: DMR-0421253.

[1]J. Chen, S. Patil, S. Seal, and J. F. McGinnis, Nat. Nanotechnol. **1**, 142 (2006).
[2]P. Mohanty and S. Ram, J. Mater. Chem. **13**, 3021 (2003).
[3]R. Reisfeld, E. Zigansky, and M. Gaft, Mol. Phys. **102**, 1319 (2004).
[4]S. Fujihara and M. Oikawa, J. Appl. Phys. **95**, 8002 (2004).
[5]X. Liu, S. Chen, and X. Wang, J. Lumin. **127**, 650 (2007).
[6]Z. Wang, Z. Quen, and J. Lin, Inorg. Chem. **46**, 5237 (2007).
[7]Z. L. Wang and X. Feng, J. Phys. Chem. B **107**, 13563 (2003).
[8]JCPDS Card No. 810792.
[9]R. D. Shannon and C. T. Prewitt, Acta Crystallogr. **B26**, 1046 (1970).
[10]S. Deshpande, S. Patil, S. V. N. T. Kuchibhatla, and S. Seal, Appl. Phys. Lett. **87**, 133113 (2006).
[11]S. Tsunekawa, T. Fukuda, and A. Kasuya, Surf. Sci. **457**, L437 (2000).
[12]E. J. Cho and S. J. Oh, Phys. Rev. B **59**, R15613 (1999).
[13]J. R. McBride, K. C. Hass, B. D. Poindexter, and W. H. Weber, J. Appl. Phys. **76**, 2435 (1994).
[14]S. Patil, S. Seal, Y. Guo, A. Schulte, and J. Norwood, Appl. Phys. Lett. **88**, 243110 (2006).
[15]S. Tsunekawa, T. Fukuda, and A. Kasuya, J. Appl. Phys. **87**, 1318 (2000).
[16]K. Li and D. Xue, Phys. Status Solidi B **244**, 1982 (2007).